Sintering of lixiviated nano glass-ceramics: An original route to elaborate transparent ceramics

Claire Mével, Julie Carreaud, Celine Caillaud, Francesco Bour, Gaelle Delaizir, Victor Castaing, Bruno Viana, Pierre Carles, François Brisset, Cécile Genevois, et al.

Sintering of lixiviated nano glass-ceramics: an original route to elaborate transparent ceramics

Claire Mével[1], Julie Carreaud[1], Céline Caillaud[1], Francesco Bour[1], Gaëlle Delaizir[1], Victor Castaing[2], Bruno Viana[2], Pierre Carles[1], François Brisset[3], Cécile Genevois[4], Mathieu Allix[4], Sébastien Chenu*[,5]

[1]*Institut de Recherche sur les Céramiques (IRCER), UMR 7315 CNRS, Université de Limoges, Centre Européen de la Céramique, Limoges, France*

[2]*Université PSL, Chimie ParisTech, CNRS, IRCP, Institut de Recherche de Chimie Paris, Paris, 75005, France*

[3]*Institut de Chimie Moléculaire et des Matériaux d'Orsay (ICMMO), UMR 8182 CNRS, Orsay, France*

[4]*Conditions Extrêmes et Matériaux : Haute Température et Irradiation (CEMHTI), UPR 3079 CNRS, Orléans, France*

[5]*Institut des Sciences Chimiques de Rennes (ISCR), UMR 6226 CNRS, Rennes, France*

*Corresponding author: sebastien.chenu@univ-rennes1.fr

Abstract

We report the elaboration of translucent $ZnGa_2O_4$ ceramics by an innovative process, the sintering by Spark Plasma Sintering (SPS) of spinel ceramic powder obtained by the lixiviation of glass-ceramics. Indeed, a selective dissolution of the silica-rich glass matrix allows isolating $ZnGa_2O_4$ nanocrystals embedded in the silicate glass-ceramic. This glass-ceramic is elaborated from the parent glass of composition 55 SiO_2 - 5 Na_2O - 17 ZnO - 23 Ga_2O_3 ($\%_{mol}$) that undergoes a subsequent heat-treatment at 1100°C under air leading to the crystallization of zinc gallate spinel nanocrystals with size in the 20-60 nm range. Lixiviated nanocrystals are

collected and sintered by SPS to get a bulk ceramic. While the transmittance of this ceramic is only 60% at 4.5µm, which is lower than the theoretical transmittance (82.5%), these first results are still promising and pave the way to new transparent ceramic processing route. Indeed, glass crystallization combined with selective lixiviation process is a powerful, non-conventional elaboration process that can further allow the stabilization and isolation of metastable crystalline phases with interesting functional properties.

Keywords: Transparent ceramic, $ZnGa_2O_4$, glass ceramic, lixiviation, nanocrystals, spinel

1. Introduction

Transparent ceramics have raised significant attention during the last decades due to their promising and remarkable combination of optical, mechanical, dielectric and thermal properties [1-7]. Transparent crystalline materials can be obtained through different synthesis routes using i) the Czochralski, Verneuil or flux growing methods for example to get high quality single crystals [8-10], ii) the sintering of nano-powders by vacuum sintering [11], hot uniaxial or isostatic pressing (HP/HIP) [12, 13] and iii) non-conventional sintering techniques like the Spark Plasma Sintering (SPS) [14, 15].

Powder sintering ceramic process is challenging for several reasons. First, most light-scattering sources arise from the ceramic's microstructure, such as pores, as well as the presence of impurities, secondary phases, and birefringence effects. Indeed, the presence of residual porosity (i.e. source of light scattering) in the final ceramic is strongly deleterious for the transparency [16]. In fact, it has been often reported that the volume of pores in such ceramics must remain smaller 100 vppm to reach photonic quality (i.e. with transmissions close to theoretical ones) [1, 5, 6]. Since 2012, an innovative process has been developed by M. Allix

et al. [17] to synthesize transparent oxide ceramics by complete crystallization of bulk glasses. Nevertheless, this method requires the vitrification of the targeted ceramic composition which is not always possible for the $ZnGa_2O_4$ spinel. This cubic zinc gallate spinel has been widely studied for optical applications such as saturable absorbers [18], in vivo bio-imaging applications [19], thermal sensors [20], X-ray dosimetry [21], optoelectronics [22], anti-counterfeiting applications [23]. Recently, this spinel material has been elaborated as transparent ceramic by combining high energy milling and SPS [15] but also using co-precipitation method and HIP [12, 24]. Secondly, the use of nanometric precursor powders with controlled granulometry and high purity requires physicochemical synthesis routes that are often time-consuming, expensive and complex to implement. Here, an innovative approach has been developed, nanopowders of $ZnGa_2O_4$ ceramic could be obtained by the lixiviation of glass-ceramics.

In the present study, we report a novel synthesis route starting from a transparent nano glass-ceramic material that undergoes, after prior comminution, a selective lixiviation or dissolution process of the glass matrix leading to obtainment of fine particles carrying separated nanocrystals. Indeed, S. Chenu et al. [25] have shown that highly transparent $ZnGa_2O_4$ glass-ceramic materials are elaborated via a simple heat treatment of a 55 SiO_2 - 5 Na_2O - 17 ZnO - 23 Ga_2O_3 parent glass composition, which presents nanoscale spinodal phase separation. This optimized glass-ceramic exhibits 50 $\%_{wt}$ of $ZnGa_2O_4$ nanocrystals showing a homogeneous and tunable size until 1200°C. After lixiviation, these spinel crystals are then used as a powder media which is sintered into a transparent ceramic material by SPS. The scheme of this process is depicted in Figure 1. Glass crystallization is indeed a powerful and non-conventional elaboration process for stabilizing novel compounds with interesting functional properties and metastable phases such as $BaAl_4O_7$ [26], nonstoichiometric garnets [27], or $La_2Ga_3O_{7.5}$ [28]. This innovative technique paves the way to new compositions of transparent ceramics that are

difficult to obtain by others common synthesis routes. Glass dissolution (or lixiviation) is highly studied in nuclear waste [29] or geological fields [30, 31] but to date no study has been reported in the field of optical materials. Influence parameters are linked to the medium used for lixiviation (composition, pH and stirring parameters) and to the composition and structure of the material to dissolve. The lixiviation is directly linked to the dissolution rate R_i (and to its efficiency), defined by the equation (1) [32]:

$$R^i = K_i \left[exp\left(\frac{-E_{aH+}}{RT}\right) a_H^{\eta H} + exp\left(\frac{-E_{aH_2O}}{RT}\right) + exp\left(\frac{-E_{aHO-}}{RT}\right) a_{HO-}^{\eta HO-} \right] \quad (1)$$

The dissolution phenomenon thus depends on the activation energies E_a associated with the acid, water, or hydroxide activated reactions, the temperature T, the chemical activities a_i and the order of the reaction related to the involved species H_3O^+, H_2O and HO^-. K_i is a constant depending on the dissolved composition. The ability of a material to be dissolved is related to i) its composition and structure (network) and ii) the environment of lixiviation *i.e* pH, temperature, stirring and renewal of the lixiviation solution.

As a proof-of-concept, a glass-ceramic from the SiO_2 - Na_2O - ZnO - Ga_2O_3 system has been chosen as it allows the crystallization at the nanometric scale of the well-known cubic spinel $ZnGa_2O_4$ [25]. $ZnGa_2O_4$ is a promising material for optical applications, due to its wide transparency window from ultraviolet to mid-IR wavelengths (0.2-9 μm) and its afterglow luminescence when doped with metal transition cations [25, 33-35]. $ZnGa_2O_4$ crystallizes in a cubic direct "AB_2O_4" spinel structure with the $Fd\bar{3}m$ space group and a lattice parameter a=8.3366 Å in which Zn^{2+} ions occupy the tetrahedral A-sites and Ga^{3+} the octahedral B-sites [36]. This material can be synthetized as single crystal [10, 37], nanocrystals [38, 39], micrometric ceramic powder [40, 41], glass ceramics [25, 34, 42], thin films [43, 44] or even nanotubes [45] but also as a transparent ceramic [12, 15, 24].

Here, we show that high crystallinity zinc gallate spinel nanocrystals could be synthesized and embedded in a glass-ceramic material. Contrary to common lixiviation studies in glass, the aim

of this work is to favor the glass matrix dissolution of a nano glass-ceramic to isolate embedded nanocrystals (Figure 1). This process is considered as a new technique to obtain nanocrystals using the natural dispersion of crystals in a nano glass-ceramic. Furthermore, the nano-powders obtained are highly crystalline depending on the heat-treatment, which may not be the case when sol-gel technique is used. The dissolution of the glass matrix is studied to recover the nanocrystals which are further used in SPS sintering experiments in order to elaborate transparent $ZnGa_2O_4$ transparent ceramics. The structure, microstructure and optical properties of the obtained transparent ceramic are studied and compared to the literature.

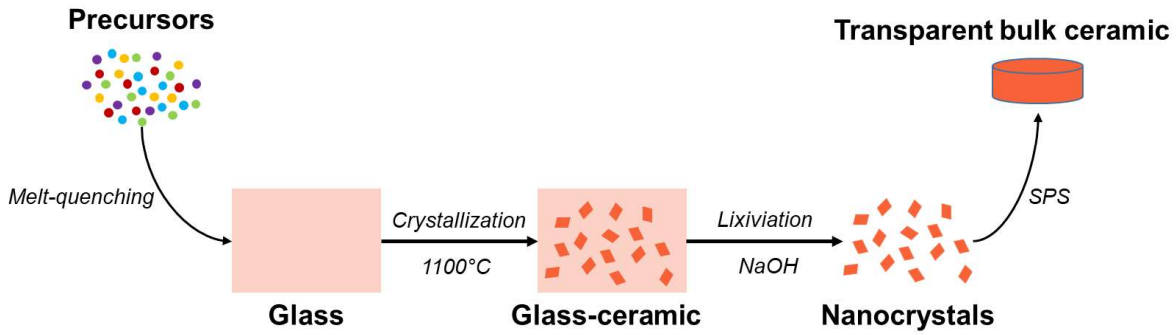

Figure 1: Scheme of the principle of the innovative synthesis way developed during this study and based on lixiviation of a nano glass-ceramic material (dissolution of the glass matrix to obtain nanocrystals sintered into a $ZnGa_2O_4$ transparent ceramic).

2. Experimental procedures

a. Synthesis

A glass composition of 55 SiO_2 - 5 Na_2O - 17 ZnO - 23 Ga_2O_3 (% mol) was prepared by the conventional melt-quenching technique as mentioned in [25]. First, the precursors (SiO_2 (Tekna), Na_2CO_3 (Aldrich, 99,95-100,05%), ZnO (Alfa Aesar, 99,99%) and Ga_2O_3 (Strem Chemicals, 99,998%)) were mixed in an agate mortar and decarbonated under air at 900°C for 6 hours. The mixture was then melted at 1600°C for 45 min under air in a platinum crucible and quenched in water. The resulting glass was crushed in an agate mortar until it passed through a 63 µm-mesh sieve and was further crystallized under air at 1100°C for 1 min in a

platinum crucible. The expected crystalline fraction in these conditions is ~ 50%$_{wt}$. Then, the glass-ceramic powder was lixiviated as followed [46]: 4g of glass ceramic powder were introduced in a 150 mL of NaOH solution, concentrated at 4 mol.L^{-1}. The solution was maintained at 95°C for 24 hours to allow the dissolution of the glass matrix. The powder was then washed by centrifugation at 1000 rpm for 10 minutes with distilled water, until the pH remained neutral. The drying of nanocrystalline powder was performed at room temperature under air.

The densification of the nanocrystalline $ZnGa_2O_4$ powders was achieved by spark plasma sintering (SPS) using a Dr.Sinter 825 Syntex machine (Fuji FDC, Japan) to obtain a transparent ceramic. The powder was introduced in an 8 mm diameter graphite die and was consolidated under vacuum at 960°C under 100 MPa. The thermo-mechanical cycle is presented in Figure 2. During the SPS process, the temperature was monitored by a thermocouple positioned through the die in the vicinity of the sample.

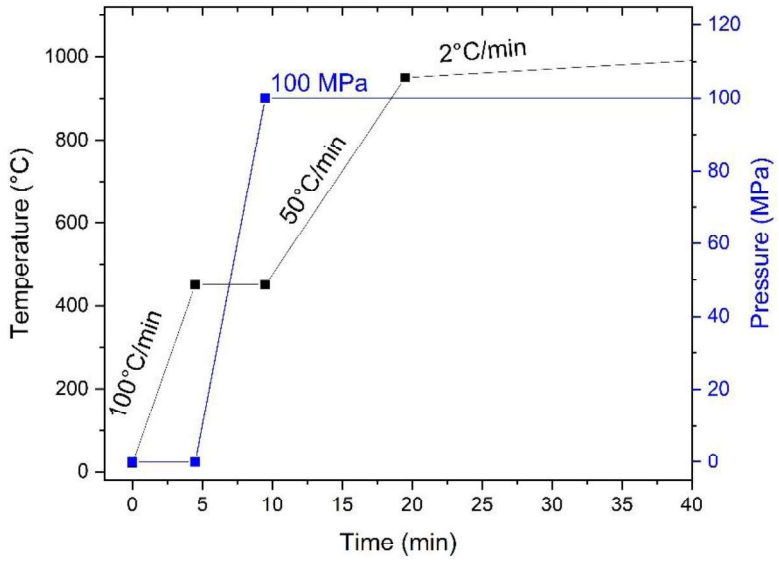

Figure 2: SPS thermo-mechanical cycle applied to sinter $ZnGa_2O_4$ nanocrystals powder (Ø 8 mm graphite die).

b. Structural characterizations

Powder X-Ray Diffraction (PXRD) data were recorded on a Bragg Brentano D8 Advance Bruker diffractometer (CuK_α radiation) equipped with a LynxEye XE detector. Short measurement range $10° < 2\theta < 70°$ was used for phase identification while Rietveld refinements were performed using a larger range ($5° < 2\theta < 130°$ with a 0.012 step size) and the JANA2020 software [47].

Scanning Electron Microscopy observations were performed using a FEG Quanta FEI device, operating at 15 kV.

Electron backscatter diffraction (EBSD) maps were recorded on the ceramic after densification by SPS, using an OIM TSL/EDAX system mounted on a FEG-SEM (Zeiss SUPRA 55 VP) system. The SEM was set with the VP mode to avoid a carbon coating and the high voltage was 30 kV. It was used to evaluate the amorphous residual parts and to visualize the microstructure of sample without chemical or thermal etching which could modify grain sizes. Before the observations, the samples were optically mirror-polished.

Transmission Electron Microscopy (TEM) was used to characterize the microstructure of the lixiviated powder and the ceramics sintered by SPS. The lixiviated powder and glass-ceramics were analyzed using a Titan Themis (200 kV, probe-corrected, probe size 0.1 nm) by TEM imaging, selected-area electron diffraction (SAED) and energy-dispersive X-ray spectroscopy (EDS) analyses. The ceramics were characterized by High-Resolution TEM (HR-TEM) and scanning transmission electron microscopy – high angle annular dark field (STEM-HAADF) imaging modes, as well as by EDS elemental mapping, using a JEOL ARM 200CF (JEOL Ltd.) cold FEG operating at 200 kV, equipped with a double spherical aberration corrector and a JEOL SDD CENTURIO EDS system. In STEM-HAADF imaging mode, a 68-174.5 mrad inner-outer collection angle and a 0.1 nm probe size were used while in EDS mapping a probe size of 0.13 nm was chosen.

The ceramics were prepared prior to (S)TEM observations by focused ion beam (FIB, ZEISS Crossbeam 550).

Optical transmission measurements were carried out within the 300-3300 nm range, with the sample placed at normal incidence, using a Varian Cary 5000 spectrophotometer operated in a dual beam configuration and in the infrared range using a Thermo Scientific Nicolet 6700 FTIR spectrophotometer.

The density of the SPS bulk samples was determined through the Archimedean principle using a Kern balance with ethanol as buoyancy media.

3. Results and discussion

Here, the lixiviation process of spinel glass-ceramics (i.e. dissolution of the silicate glass matrix) is studied to recover the nanocrystals which are further used in SPS sintering experiments in order to elaborate transparent $ZnGa_2O_4$ ceramics. Before this lixiviation steps, an adequate nano glass-ceramic is synthesized. S. Chenu et al. [25] have previously reported that 55 SiO_2 - 5 Na_2O - 17 ZnO - 23 Ga_2O_3 glass crystallizes with 50%$_{wt}$ $ZnGa_2O_4$ nanocrystals (crystallite size ~ 30 nm) using a heat treatment at 1000°C for 10 min. The process is the following; the glass exhibits a nanoscale spinodal phase separation with regions rich in i) SiO_2 and ii) ZnO and Ga_2O_3. As the size of the phase separation can be tailored via the nominal glass composition, the control of the crystal size in the glass-ceramic material is made easier via designing the phase separation size in the parent glass. The later region will transform into crystalline $ZnGa_2O_4$ at higher temperature while the region with a high silica content will remain amorphous even at high temperatures (until 1200°C) and will limit the spinel crystals growth. By this method a fraction of about 50%$_{wt}$ of the glass crystallizes forming $ZnGa_2O_4$ nanocrystals as describe below.

Figure 3-a shows the XRD patterns of the glass-ceramic powder heat-treated at 1100°C for 30s to 1h. These temperature and duration have been chosen according to previous studies [25] as a good compromise to get high crystallized fraction, homogeneous and controlled crystallite size and high crystallinity degree.

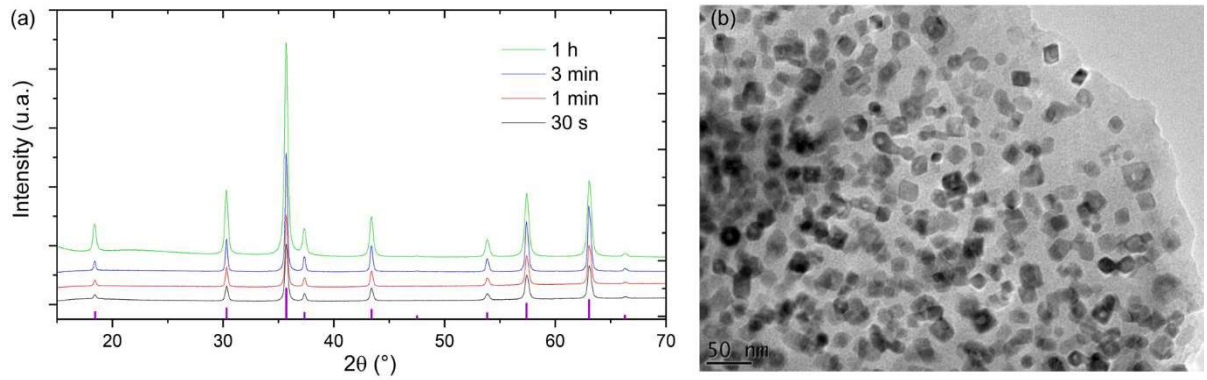

Figure 3: (a) XRD patterns of glass-ceramics heat-treated under air at 1100°C for 30 seconds (black), 1 minute (red), 3 minutes (blue) and 1 hour (green) (purple tick marks represent $ZnGa_2O_4$, JCPDS 71-0643). (b) TEM picture of glass-ceramic powder heat-treated at 1100°C for 1 min under air.

Even after only 30 s, some crystallization peaks appear in the diffractogram that well indexed by the spinel $ZnGa_2O_4$ phase which is in good agreement with the study of Chenu et al. [25]. SEM observations of the glass-ceramic powder heat-treated at 1100°C for 1 min reveal some heterogeneous agglomerated particles of few micrometers, each particle exhibiting a glass matrix with embedded $ZnGa_2O_4$ cubic crystals measuring few tens of nanometers as shown in Figure 3-b. As the duration or temperature of crystallization increases, the size of crystals slightly increases. The crystalline fraction with this specific heat-treatment is around 50 % $_{wt}$.

The glass-ceramic powder was then lixiviated according to the protocol explained in [46] and described in the experimental part to isolate $ZnGa_2O_4$ nano-crystals.

The microstructure of the lixiviated powder evidences the presence of grains that become porous after the lixiviation step as evidenced by SEM observations (Figure 4a and b), this is in favor of the dissolution of the glass matrix. These grains mainly consist of cubic nanoparticles of size between 20-60 nm (Figure 4-d and e). The inset Selected Area Electron Diffraction (SAED) pattern (Figure 4-e) evidenced bright spots which superimpose discrete diffraction

rings matching the $ZnGa_2O_4$ spinel structure and attesting the good crystallinity of the material. One can observe the presence of an amorphous shell around some $ZnGa_2O_4$ nanocrystals as shown by yellow arrows in Figure 4e. EDS-TEM and EDS-SEM analyzes (Table 1), made on lixiviated powder, highlight the presence of SiO_2 in the sample (3.8% mol.) which corresponds to amorphous SiO_2 at the surface of $ZnGa_2O_4$ nanocrystals (Table 1). The presence of this residual amorphous phase may not be detrimental to the later sintering process as it could act as sintering aid [48-51]. The particle size distribution of the lixiviated powder is shown in Figure 4-c. The distribution is multi-modes with a median diameter D_{50}=1.18 µm. The first mode centered around 0.15 µm corresponds to single particles and small agglomerates of few particles while the 2nd and 3rd modes centered around 1.5 µm and 15 µm respectively correspond both to larger agglomerates that are in good agreement with SEM observations (Figure 4a). The use of sonification and dispersant are not efficient to break the agglomerates which means that the $ZnGa_2O_4$ nanoparticles may be still linked together by the residual glass matrix.

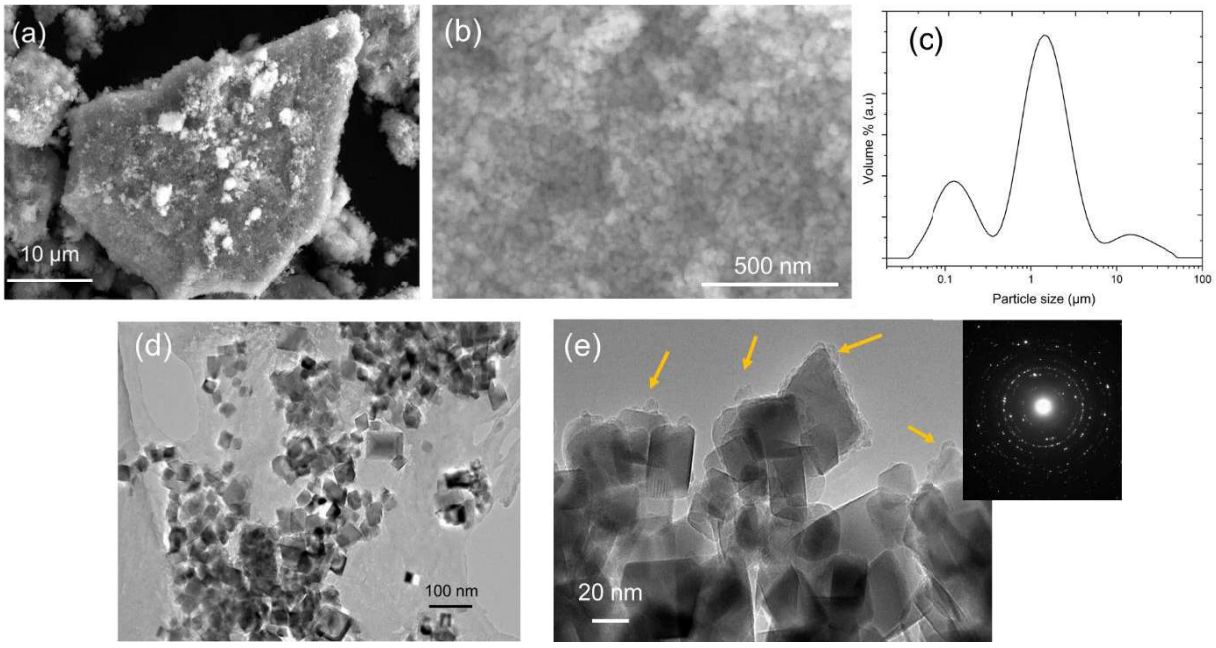

Figure 4: (a) and (b) Lixiviated $ZnGa_2O_4$ powder observed by SEM. (c) Particle size distribution of the lixiviated powder. (d) and (e) TEM and SAED pattern shown in insert

Table 1: EDS-SEM measurement performed on the glass-ceramic and the lixiviated powder (standard deviation ± 1 mol%).

	SiO_2 (%mol)	ZnO (%mol)	Ga_2O_3 (%mol)
Glass ceramic (nominal)	57.9	17.9	24.2
Glass ceramic (experimental)	58.5	16.9	24.6
Lixiviated powder	3.8	47.5	48.7
$ZnGa_2O_4$ (theoretical)	-	50	50

As the glass matrix dissolution of the glass-ceramic could lead to the partial decomposition of the zinc gallate spinel nano-crystals, XRD measurements have been performed on the resulting crystals. No changes in the XRD patterns are discernable as shown in Figure SI 1. A Rietveld refinement has been performed on the lixiviated powder (Figure SI 2). It shows that (i) no decomposition of $ZnGa_2O_4$ occurred and (ii) the average crystalline size, 56 nm, remains the same as before lixiviation. These results, in good agreement with TEM observations showing sharp edges (Figure 4-d), demonstrate that the nanocrystals were not damaged during the lixiviation process. A quantification of the amorphous phase content has been attempted using ZnO as an internal standard (Figure SI 2). This led to almost no amorphous phase detection, which, considering the error on the quantification, shows that very few amorphous phase (SiO_2) remains in the final nanoceramic.

In order to obtain a dense $ZnGa_2O_4$ ceramic, the lixiviated powder was then sintered by SPS according to the thermo-mechanical cycle depicted in Figure 2. XRD measurement confirms the conservation of the zinc gallate spinel phase after SPS sintering (Figure SI 2).

EDS-SEM analyzes, made on SPS-sintered ceramic, reveal the presence of a small amount of silicon that could be found as SiO_2 in the SPS sample (~ 0.8% at of Si) as depicted in Figure 5-c. One can note that the Ga_2O_3/ZnO ratio in $ZnGa_2O_4$ ceramic is equal to one while in the overall glass-ceramic material, it is note the case (ratio=1.35). As explained in [25], during the crystallization process, a phase separation with enriched amorphous gallium oxide appears in the residual glass and allows to obtain pure $ZnGa_2O_4$ glass-ceramic. The percentages of Zn and Ga in the SPS sample are consistent with the formation of the $ZnGa_2O_4$ cubic phase.

To have a better understanding of the microstructure of the SPS $ZnGa_2O_4$ ceramic, SEM measurements as well as EDS-SEM were acquired on a fresh fracture and a polished sample respectively. As presented in Figure 5-a, we can highlight the presence of a complex and heterogeneous microstructure with two different features. Grains of around 1 µm in size are surrounded by smaller ones as shown in Figure 6a. EDS-SEM measurements (table in Figure 5-c) reveal that the big grains show a $ZnGa_2O_4$ composition while the domains including the small grains are constituted by $ZnGa_2O_4$ associated with a small quantity of silicon (0.5 to 1%$_{at}$ Si). This Si quantity is small and the accuracy concerning this value is relatively high, nevertheless the presence of silicon is attested. SiO_2 is a well-known sintering aid for the densification of transparent ceramic, YAG for example [51, 52]. Its addition usually promotes densification, elimination of pores and grain growth either through the presence of a liquid phase, or by other mechanisms by enhancing diffusion during thermal treatments. Interestingly, in our study, the SiO_2-enriched domains are characterized by inhibited grain growth as shown in Figure 6a. This result could be explained by low sintering temperature (960°C) at which SiO_2 is not liquid (in contrary to much higher sintering temperatures of YAG) and the low solubility of $ZnGa_2O_4$ into amorphous SiO_2 at such temperature prevents grain coalescence and crystal growth. Furthermore, Si is not uniformly distributed in the ceramic while Zn and Ga seem to be distributed homogeneously. Electron backscattering diffraction (EBSD) map was recorded on

the $ZnGa_2O_4$ SPS ceramic (Figure 5d). The crystalline domains show random orientations as illustrated by pole figures (Figure 5e) and their size evolves from 100 to 600 nm, with an average size of 200 nm. The black (non-indexed) areas may attest the presence of glass phase at grain boundary and/or zones with very small grains that are not detectable. This point will be discussed in the following part of the paper.

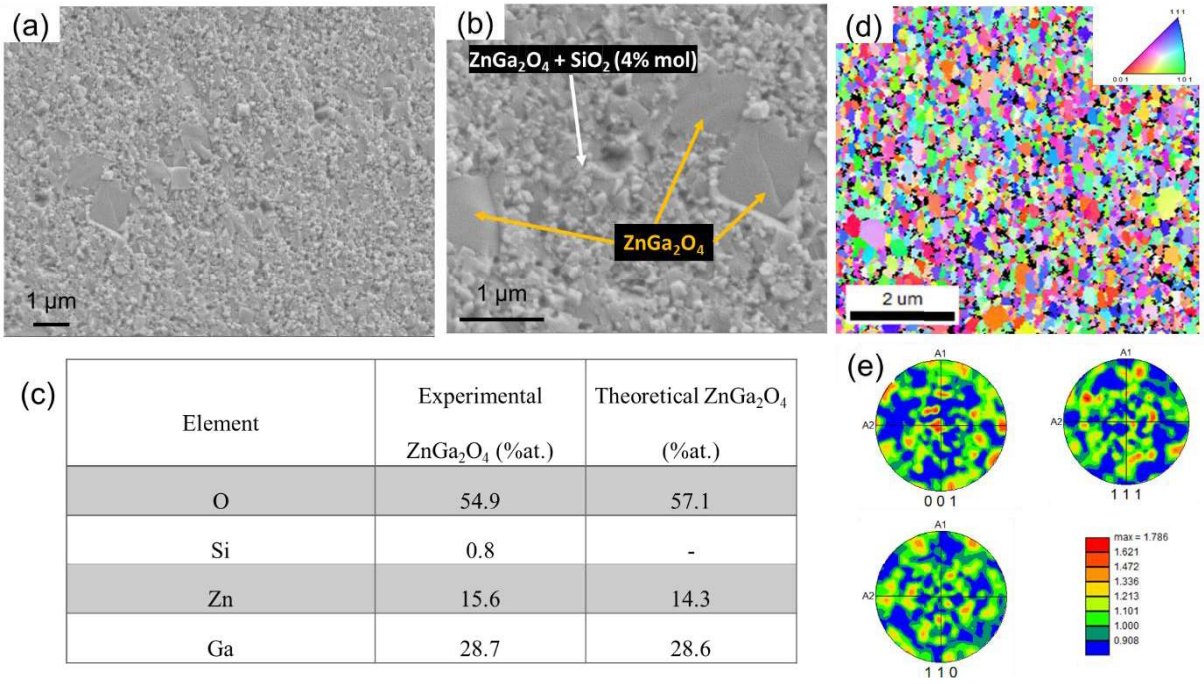

(c)

Element	Experimental $ZnGa_2O_4$ (%at.)	Theoretical $ZnGa_2O_4$ (%at.)
O	54.9	57.1
Si	0.8	-
Zn	15.6	14.3
Ga	28.7	28.6

Figure 5: SEM micrographs of SPS fresh fracture at low magnification (a) and high magnification (b). (c) EDS-SEM measurement performed on the $ZnGa_2O_4$ transparent ceramic obtained by SPS densification of lixiviated zinc gallate spinel nanocrystals (standard deviation ± 1 at%). (d) EBSD-SEM orientation map of the ceramic showing crystalline domains. (e) Pole figures showing texture in $ZnGa_2O_4$ ceramic.

To go further in the understanding of the microstructure TEM observations of the SPS $ZnGa_2O_4$ ceramics were performed on a FIB-prepared thin foil. Low magnification observations reveal that the sample is dense as no porosity is observed (Figure SI 3). STEM-HAADF (Z-contrast) imaging clearly shows a chemical contrast with two different phases: crystals with a bright contrast are surrounded by darker, i.e. a lighter phase at the grain boundaries (Figure 6c). It is noteworthy that no porosity is visible even at high magnification. The particle size distribution calculated on more than 500 grains is in the range 10-160 nm, the average size and the standard deviation are around 57 nm and 26 nm respectively (Figure 6b). STEM-EDS elemental map and

punctual analyzes reveal that the lighter phase is only composed of SiO_2 while the composition of the grains is $ZnGa_2O_4$ (Figure 6d). The HRTEM images taken on different location of the FIB prepared sample exhibit different types of grain boundaries. First, it is important to highlight that the SiO_2 phase at the grain boundaries is amorphous. Indeed, the FFT indexations of the crystals and surrounded phase are consistent with both a cubic spinel phase structure and amorphous phase, respectively (Figure 6-d). The amorphous SiO_2 phase that remains after incomplete lixiviation process of the glass-ceramic can be found as domains of few tens of nm that fill the porosities which is of great importance especially for optical properties (i.e. diminution of light scattering). One also can note that the amorphous SiO_2 phase is localized on thin edges between $ZnGa_2O_4$ grains (yellow arrows in Figure 6) which prevents from grain growth and enhances mechanical properties. Some thin boundaries (~ 2 nm) between two crystals and without any glass at the interface are also evidenced in the sample (Figure 6-f). Indeed, at some point and when no amorphous phase is detected at the grain boundaries, the coalescence phenomenon leading to grain growth takes place as illustrated in Figure 6-g, where we can see on the HRTEM image and the associated FFT that the (111) plans of two grains are in the process of aligning with each other to become finally one grain. An attempt to estimate the amount of amorphous phase has been performed by assuming that (i) the amorphous phase is only made of pure SiO_2 glass and (ii) the crystals are made of pure $ZnGa_2O_4$ with no Si. With such hypotheses, the amount of amorphous phase, measured on a ≈1 μm^2 area, is estimated to ~ 6% mol which is in the same range of the content found by EDS-SEM (~ 5% mol i.e. ~ 2.3% $_{wt}$).

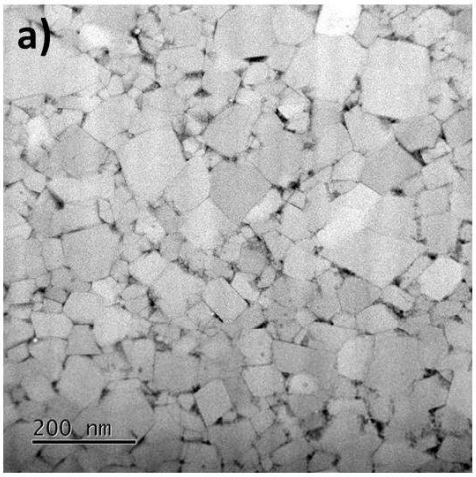

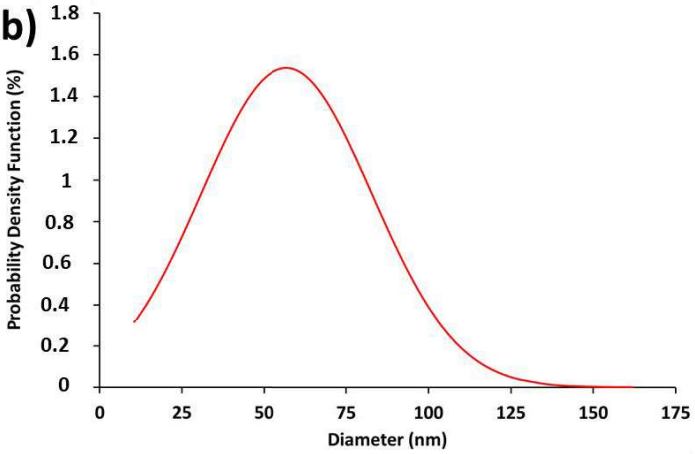

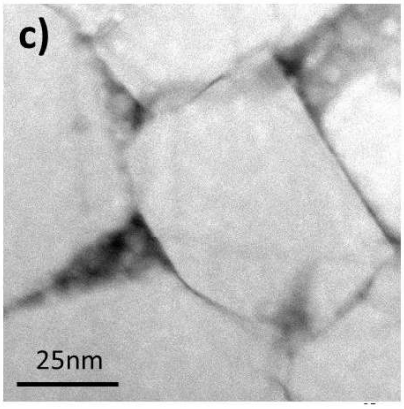

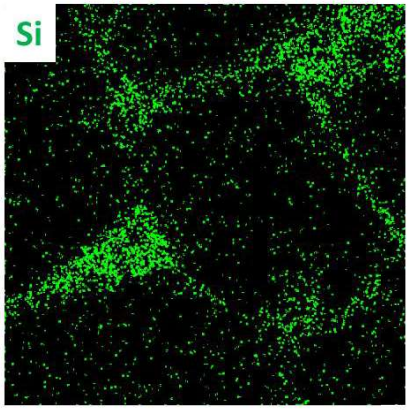

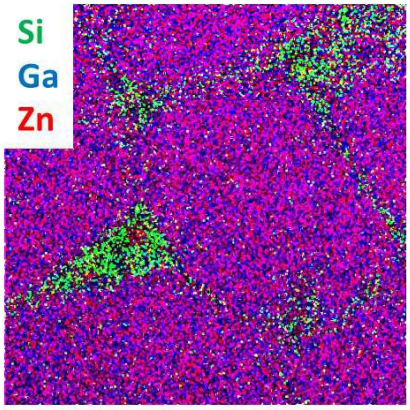

FFT grain

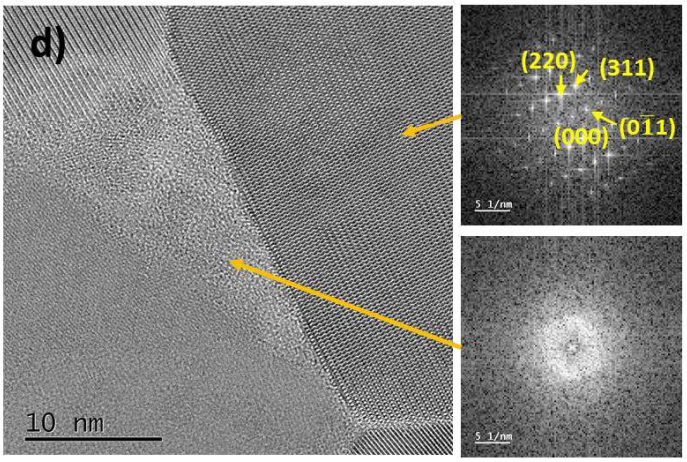

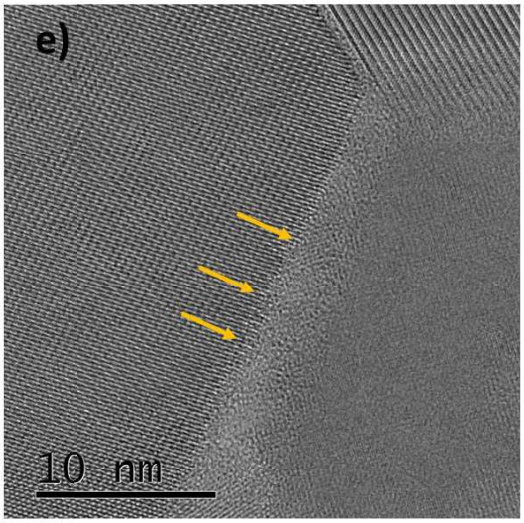

FFT glass

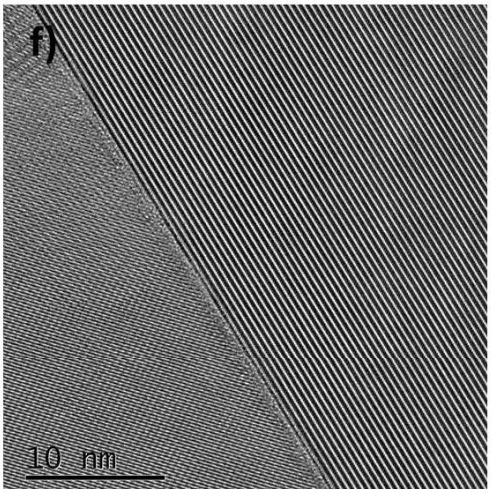

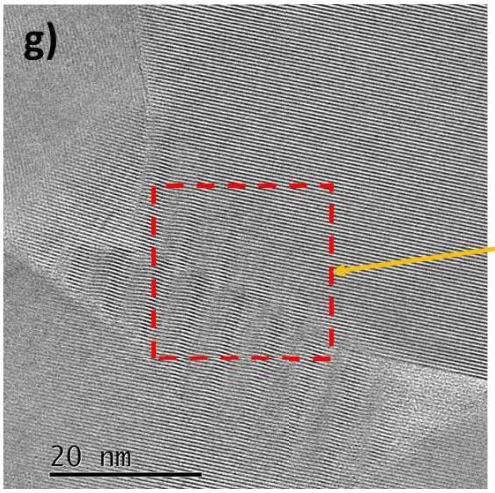

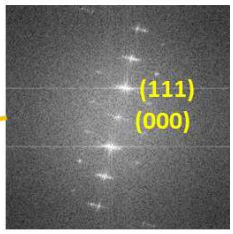

FFT

Figure 6: $ZnGa_2O_4$ SPS ceramic (a) STEM-HAADF image of FIB lamella, (b) Grain-size distribution performed on more than 500 crystals, (c) STEM-EDS elemental maps (d) STEM-EDS (d), (e), (f), (g) (e), (f), (g), HRTEM images and associated FFT showing different types of grain boundaries.

Finally, the transmittance of the SPS sintered sample was measured. The resulting $ZnGa_2O_4$ ceramic is translucent and exhibits a density of 5.93 $g.cm^{-3}$ leading to a compactness of 99.8% considering a density of 6.15 $g.cm^{-3}$ for $ZnGa_2O_4$ and the presence of ~ 5% mol of pure SiO_2 as observed by EDS. This result is in good agreement with the TEM observations (Figure 6-a) where no porosity is detectable. One may confirm that a residual glass phase contributes to the density. Some black spots that are characteristics of carbon contamination due to the use of graphite environment [15, 53] are observable in the sample (Figure 7). This contamination has already been oberved in $ZnGa_2O_4$ samples and others transparent materials sintered by SPS [15, 54, 55]. In some cases, after this SPS step, a post annealing treatment in air was performed to remove carbon contamination [14, 56]. The transmission window extends from 0.7 µm to 8.5 µm. Absorption bands at 2 µm, 3.1 µm, 5.5 µm and after 7.2 µm are observed on the different transmittance spectra. The broad band located around 3 µm is due to the presence of free hydroxyl groups probably exacerbated by the lixiviation media [57]. It is noteworthy that the other bands are absent in the study made by C. Mével *et al*. [15] who prepared transparent $ZnGa_2O_4$ ceramic by ball-milling from nanometric and micrometric precursors and subsequent SPS sintering. These extra bands can thus be associated to the presence of a small amount of silica in the ceramic sample [58]. This amorphous SiO_2 residual part could be found around the nanocrystals of zinc gallate spinel as shown by TEM observations (Figure 4-e) and may result from an incomplete lixiviation process. The maximum of transmittance is ~ 60% at 4.5 µm. This value is far from the theoretical value calculated on a $ZnGa_2O_4$ single crystal (82.5% at 2 µm) but this result can be explained by different parameters. First and even if the amount of amorphous silica is low and the size of the amorphous domains is small (from few nm to few tens of nm) and acts as a sintering aid by closing the intergranular positites, its refractive index (1.45 at 1µm) is very different from the one of $ZnGa_2O_4$ (1.97 at 1µm) and may induce some

light scattering [16]. Then the carbon contamination is also a source of scattering [53]. As the $ZnGa_2O_4$ spinel is a cubic structure, the grain size is not a detrimental parameter for transmittance but the starting powder is made of agglomerates with different sizes as shown in Figure 4-a that affects the sinterability and thus the optical properties of the final ceramic [59, 60]. Future work will attempt to enhance the transparency of the final ceramic by preventing carbon contamination. Indeed, the lixiviated powder should be sintered without graphitic environment by combining pressureless and a hot isostatic sintering [3].

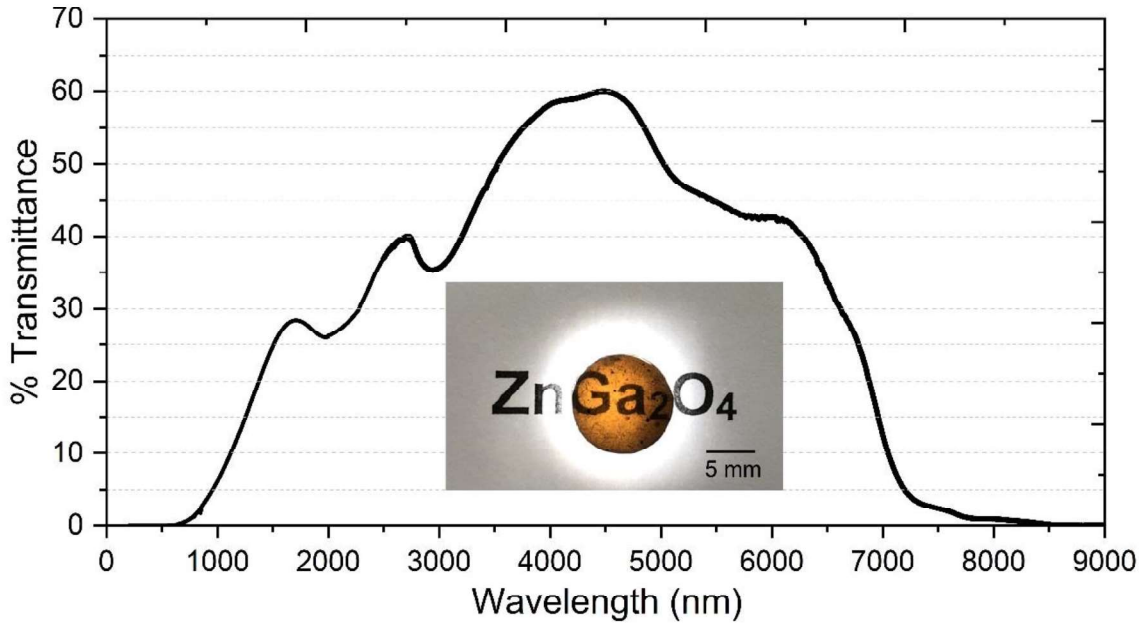

Figure 7 : Transmittance spectra of as-SPS sample (thickness: 1.2 mm) and photograph of SPS $ZnGa_2O_4$ translucent ceramic (Ø 8mm).

4. Conclusion

We reported on a detailed investigation of the innovative synthesis, microstructure and optical properties of $ZnGa_2O_4$ translucent ceramics. Nanocrystalline zinc gallate spinel powder was obtained by an original process based on the glass-ceramic lixiviation. First, a parent glass of composition 55 SiO_2 - 5 Na_2O - 17 ZnO - 23 Ga_2O_3 ($\%_{mol}$) was synthetized by conventional melt quenching technique and, after milling, was crystallized at 1100°C for 1 min. The resulting

glass-ceramic with a $ZnGa_2O_4$ crystalline fraction of ~50%$_{wt.}$ was then lixiviated in a basic media to dissolve selectively the glass matrix. The $ZnGa_2O_4$ crystalline nano-powder (20-60 nm) was then recovered by centrifugation, dried and densified by Spark Plasma Sintering. We showed that some residual amorphous silica part that comes from the slightly incomplete lixiviation process, surrounds some $ZnGa_2O_4$ grains. A transmittance of 60% at 4.5µm is obtained in the best ceramic sample.

The use of glass-ceramic lixiviation to obtain a powder of high crystalline nanocrystals was never reported before in the literature. This innovative approach constitutes a real breakthrough in the field of nanometric powder preparation, as it allows a highly crystalline nano powder to be obtained, which is usually not the case with sol-gel technique for example.

Moreover, it is well-known that glass ceramics enable the stabilization of novel and metastable phases. Therefore, this technique could be used to further synthetize new metastable powders that cannot be obtained by common solid-state synthesis routes.

Acknowledgements

This work was supported by institutional grants from LabEX SigmaLim (ANR-10-LABX-0074-01). This work has benefited from the electron microscopy facilities of the Platform MACLE-CVL, which was cofounded by the European Union and Centre-Val de Loire Region (FEDER). The authors would like to thank the NEMATUUM project (AAP NA 2017-1R50313) for its financial support.

Electronic Supplementary Material

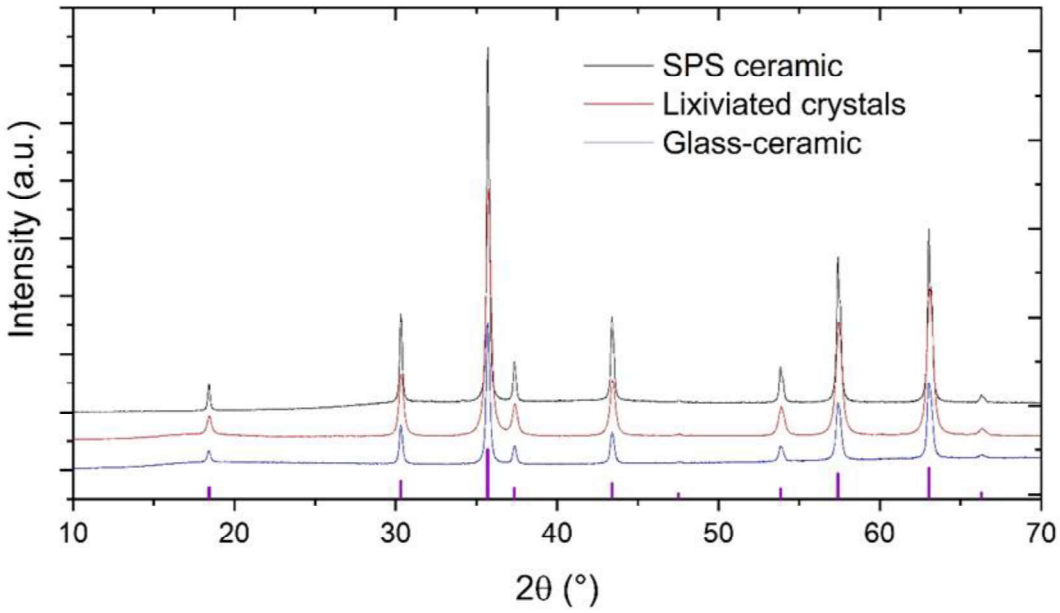

Figure SI 1: XRD patterns of the glass-ceramic heat-treated at 1100°C for 1 min, the corresponding lixiviated powder and the SPS ceramic sintered from lixiviated powder. The $ZnGa_2O_4$ indexations (JCPDS 71-0643) are indicated below in purple.

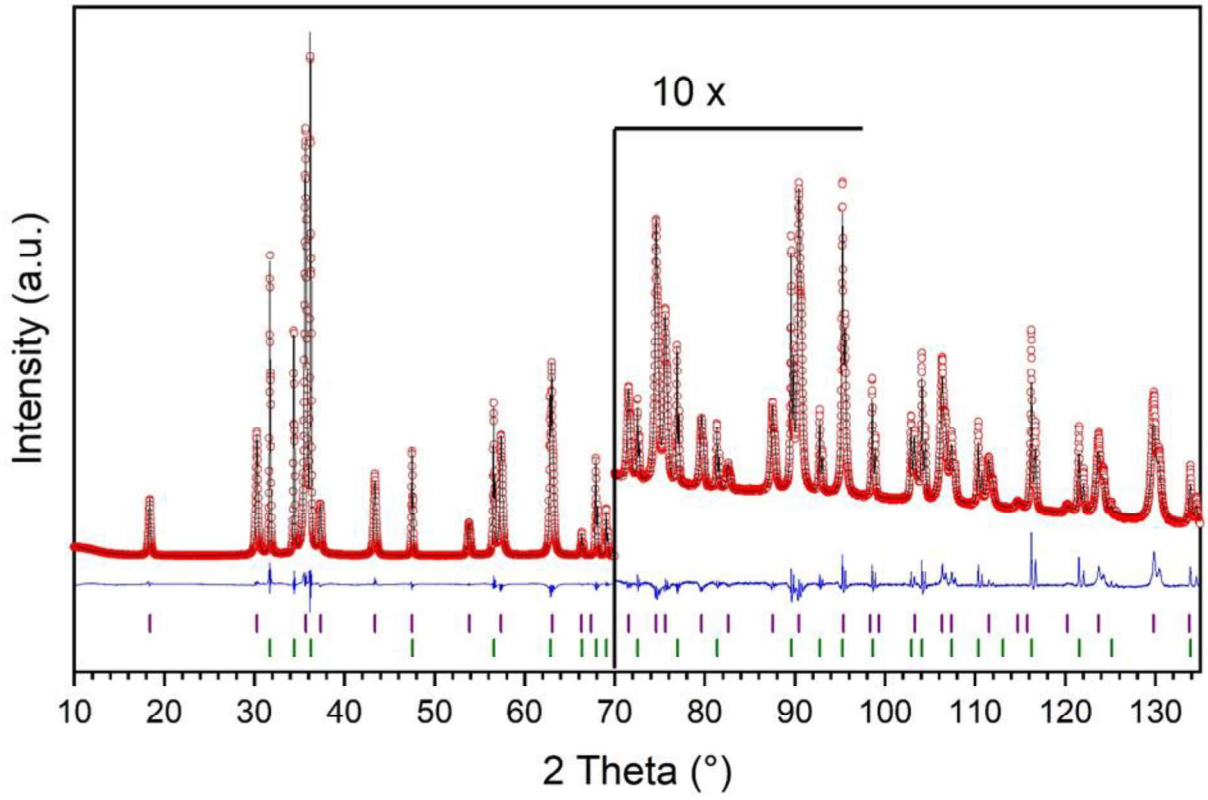

Figure SI 2: Rietveld refinement of lixiviated $_{ZnGa2O4}$ glass-ceramic powder. Black circles, red and blue solid lines, vertical purple and green ticks correspond to experimental data, simulated diagram, difference curve and indexation of $ZnGa_2O_4$ and ZnO (added internal standard for amorphous phase quantifications), respectively. The diffractogram above 70° has been scaled up (x10) for better appreciating the fit. Reliability factors are wRP = 4.20 %, Rp = 3.08 % and GOF = 7.33 .

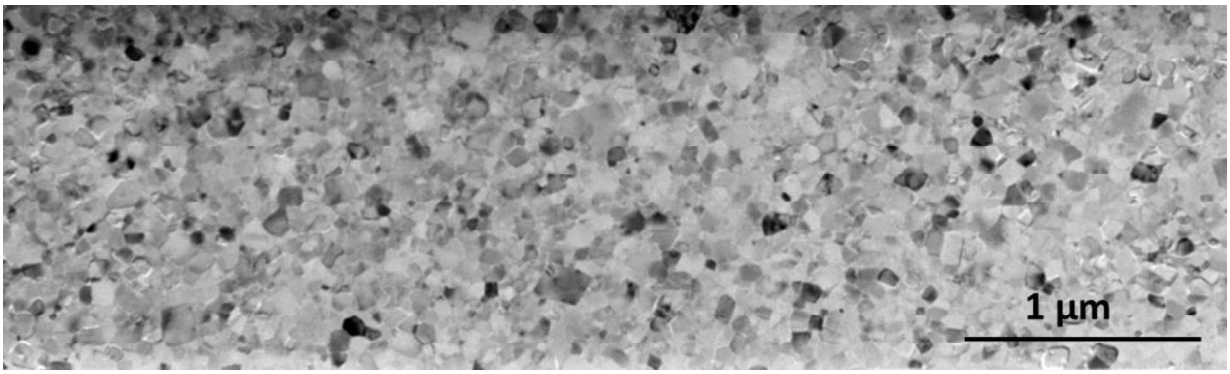

Figure SI 3: TEM image of the FIB lamella overview of $ZnGa_2O_4$ SPS ceramic

References

[1] L.B. Kong, Y.Z. Huang, W.X. Que, T.S. Zhang, S. Li, J. Zhang, Z.L. Dong, D.Y. Tang, Transparent Ceramics, Springer International Publishing2015.

[2] G. Partridge, Inorganic materials IV. Transparent ceramics and glass-ceramics, Adv. Mater. 2(11) (1990) 553-556.

[3] S.F. Wang, J. Zhang, D.W. Luo, F. Gu, D.Y. Tang, Z.L. Dong, G.E.B. Tan, W.X. Que, T.S. Zhang, S. Li, L.B. Kong, Transparent ceramics: Processing, materials and applications, Prog. Solid State Chem. 41(1–2) (2013) 20-54.

[4] U. Jumpei, K. Keisuke, T. Setsuhisa, Yellow persistent luminescence in Ce^{3+}–Cr^{3+} -codoped gadolinium aluminum gallium garnet transparent ceramics after blue-light excitation, Applied Physics Express 7(6) (2014) 062201.

[5] A. Ikesue, Y.L. Aung, Ceramic laser materials, Nature Photonics 2(12) (2008) 721-727.

[6] G.L. Messing, A.J. Stevenson, Toward pore-free ceramics, Science 322(5900) (2008) 383-384.

[7] N. Martin, Y. Akira, Recent R&D Trends in Inorganic Single-Crystal Scintillator Materials for Radiation Detection, Advanced Optical Materials 3(4) (2015) 463-481.

[8] P.S. Dutta, 3.02 - Bulk Growth of Crystals of III–V Compound Semiconductors, in: P. Bhattacharya, R. Fornari, H. Kamimura (Eds.), Comprehensive Semiconductor Science and Technology, Elsevier, Amsterdam, 2011, pp. 36-80.

[9] Z. Galazka, D. Klimm, K. Irmscher, R. Uecker, M. Pietsch, R. Bertram, M. Naumann, M. Albrecht, A. Kwasniewski, R. Schewski, M. Bickermann, $MgGa_2O_4$ as a new wide bandgap transparent semiconducting oxide: growth and properties of bulk single crystals, physica status solidi (a) 212(7) (2015) 1455-1460.

[10] Z. Galazka, S. Ganschow, R. Schewski, K. Irmscher, D. Klimm, A. Kwasniewski, M. Pietsch, A. Fiedler, I. Schulze-Jonack, M. Albrecht, T. Schröder, M. Bickermann, Ultra-wide bandgap, conductive, high mobility, and high quality melt-grown bulk $ZnGa_2O_4$ single crystals, APL Materials 7(2) (2019) 022512.

[11] T. Epicier, G. Boulon, W. Zhao, M. Guzik, B. Jiang, A. Ikesue, L. Esposito, Spatial distribution of the Yb^{3+} rare earth ions in $Y_3Al_5O_{12}$ and Y_2O_3 optical ceramics as analyzed by TEM, J. Mater. Chem. 22(35) (2012) 18221-18229.

[12] B. Wang, H. Wang, B. Tu, K. Zheng, H. Gu, W. Wang, Z. Fu, Optical transmission, dispersion, and transition behavior of $ZnGa_2O_4$ transparent ceramic, J. Am. Ceram. Soc. 106(2) (2022) 1-10.

[13] C. Chlique, O. Merdrignac-Conanec, N. Hakmeh, X. Zhang, J.-L. Adam, Transparent ZnS Ceramics by Sintering of High Purity Monodisperse Nanopowders, J. Am. Ceram. Soc. 96(10) (2013) 3070-3074.

[14] J. Carreaud, J.-R. Duclere, Y. Launay, N. Tessier-Doyen, D.S. Smith, M. Allix, V. Couderc, G. Delaizir, S. Chenu, Fabrication and optical properties of transparent fine-grained $Zn_{1.1}Ga_{1.8}Ge_{0.1}O_4$ and Ni^{2+} (or Cr^{3+})-doped $Zn_{1.1}Ga_{1.8}Ge_{0.1}O_4$ spinel ceramics, J. Eur. Ceram. Soc. 43 (2023) 4976-4984.

[15] C. Mével, J. Carreaud, G. Delaizir, J.-R. Duclère, F. Brisset, J. Bourret, P. Carles, C. Genevois, M. Allix, S. Chenu, First $ZnGa_2O_4$ Transparent Ceramics, J. Eur. Ceram. Soc. 41(9) (2021) 4934-4941.

[16] R. Apetz, M.P.B. van Bruggen, Transparent alumina: A light-scattering model, J. Am. Ceram. Soc. 86(3) (2003) 480-486.

[17] I. Milisavljevic, M.J. Pitcher, J. Li, S. Chenu, M. Allix, Y. Wu, Crystallization of glass materials into transparent optical ceramics, Int. Mater. Rev. (2022) 1-29.

[18] P. Loiko, O.S. Dymshits, V.V. Vitkin, N.A. Skoptsov, A.A. Zhilin, D.V. Shemchuk, M.Y. Tsenter, K. Bogdanov, A.M. Malyarevich, I.V. Glazunov, X. Mateos, K.V. Yumashev, Saturable absorber: transparent glass-ceramics based on a mixture of Co:B-Zn_2SiO_4 and Co:ZnO nanocrystals, Appl. Opt. 55(21) (2016) 5505-5512.

[19] T. Maldiney, A. Bessière, J. Seguin, E. Teston, S.K. Sharma, B. Viana, A.J.J. Bos, P. Dorenbos, M. Bessodes, D. Gourier, D. Scherman, C. Richard, The in vivo activation of persistent nanophosphors for optical imaging of vascularization, tumours and grafted cells, Nat Mater 13(4) (2014) 418-426.

[20] E. Glais, M. Pellerin, V. Castaing, D. Alloyeau, N. Touati, B. Viana, C. Chanéac, Luminescence properties of $ZnGa_2O_4:Cr^{3+},Bi^{3+}$ nanophosphors for thermometry applications, RSC Advances 8(73) (2018) 41767-41774.
[21] A. Luchechko, Y. Zhydachevskyy, S. Ubizskii, O. Kravets, A.I. Popov, U. Rogulis, E. Elsts, E. Bulur, A. Suchocki, Afterglow, TL and OSL properties of Mn^{2+}doped $ZnGa_2O_4$ phosphor, Scientific Reports 9(1) (2019) 9544.
[22] E. Chikoidze, C. Sartel, I. Madaci, H. Mohamed, C. Vilar, B. Ballesteros, F. Belarre, E. del Corro, P. Vales-Castro, G. Sauthier, L. Li, M. Jennings, V. Sallet, Y. Dumont, A. Pérez-Tomás, p-Type Ultrawide-Band-Gap Spinel $ZnGa_2O_4$: New Perspectives for Energy Electronics, Crystal Growth & Design (2020).
[23] C. Ma, H. Liu, F. Ren, Z. Liu, Q. Sun, C. Zhao, Z. Li, The Second Near-Infrared Window Persistent Luminescence for Anti-Counterfeiting Application, Crystal Growth & Design 20(3) (2020) 1859-1867.
[24] Q. Liu, X. Mao, X. Li, P. Chen, X. Liu, Z. Liu, D. Zhu, H. Chen, T. Xie, J. Li, Fabrication and characterizations of Cr^{3+} doped $ZnGa_2O_4$ transparent ceramics with persistent luminescence, J. Am. Ceram. Soc. 104(10) (2021) 4927-4931.
[25] S. Chenu, E. Veron, C. Genevois, G. Alain, G. Matzen, M. Allix, Long-lasting luminescent $ZnGa_2O_4:Cr^{3+}$ transparent glass-ceramics, Journal of Materials Chemistry C 2 (2014) 10002-10010.
[26] M. Allix, S. Alahrache, F. Fayon, M. Suchomel, F. Porcher, T. Cardinal, G. Matzen, Highly Transparent $BaAl_4O_7$ Polycrystalline Ceramic Obtained by Full Crystallization from Glass, Adv. Mater. 24(41) (2012) 5570-5575.
[27] W. Cao, A.I. Becerro, V. Castaing, X. Fang, P. Florian, F. Fayon, D. Zanghi, E. Veron, A. Zandonà, C. Genevois, M.J. Pitcher, M. Allix, Highly Nonstoichiometric YAG Ceramics with Modified Luminescence Properties, Adv. Funct. Mater. 33(14) (2023) 2213418.
[28] J. Fan, V. Sarou-Kanian, X. Yang, M. Diaz-Lopez, F. Fayon, X. Kuang, M.J. Pitcher, M. Allix, $La_2Ga_3O_{7.5}$: A Metastable Ternary Melilite with a Super-Excess of Interstitial Oxide Ions Synthesized by Direct Crystallization of the Melt, Chem. Mater. 32(20) (2020) 9016-9025.
[29] B. Grambow, Nuclear waste glass dissolution: Mechanism, model and application, Sweden, 1987, p. 121.
[30] P.V. Brady, J.V. Walther, Controls on silicate dissolution rates in neutral and basic pH solutions at 25°C, Geochim. Cosmochim. Acta 53(11) (1989) 2823-2830.
[31] P.V. Brady, J.V. Walther, Kinetics of quartz dissolution at low temperatures, Chem. Geol. 82 (1990) 253-264.
[32] D. Strachan, Glass dissolution asa function of pH and its implications for understanding mechanisms and future experiments, Geochim. Cosmochim. Acta 219 (2017) 111-123.
[33] P. Zhang, Z. Luo, S. Liu, W. Lei, H. Liang, Z. Zhou, A. Lu, Crystallization kinetics and optical properties of transparent glass-ceramics embedding $ZnGa_2O_4$ nanocrystals with enhanced defect luminescence, J. Non-Cryst. Solids 576 (2022) 121255.
[34] S. Chenu, E. Véron, C. Genevois, G. Matzen, T. Cardinal, A. Etienne, D. Massiot, M. Allix, Tuneable Nanostructuring of Highly Transparent Zinc Gallogermanate Glasses and Glass-Ceramics, Advanced Optical Materials 2(4) (2014) 364-372.
[35] M. Jin, F. Li, J. Xiahou, L. Zhu, Q. Zhu, J.-G. Li, A new persistent luminescence phosphor of $ZnGa_2O_4:Ni^{2+}$ for the second near-infrared transparency window, J. Alloys Compd. 931 (2023) 167491.
[36] J. Hornstra, E. Keulen, Oxygen parameter of spinel $ZnGa_2O_4$, Philips Research Reports 27(1) (1972) 76.
[37] J. Boy, M. Handwerg, R. Mitdank, Z. Galazka, S.F. Fischer, Charge carrier density, mobility, and Seebeck coefficient of melt-grown bulk $ZnGa_2O_4$ single crystals, AIP Advances 10(5) (2020) 055005.
[38] X. Duan, J. Liu, Y. Wu, F. Yu, X. Wang, Structure and luminescent properties of Co^{2+}/Cr^{3+} co-doped $ZnGa_2O_4$ nanoparticles, J. Lumin. 153 (2014) 361-368.
[39] H.-J. Byun, J.-U. Kim, H. Yang, Blue, green, and red emission from undoped and doped $ZnGa_2O_4$ colloidal nanocrystals, Nanotechnology 20(49) (2009) 495602.
[40] M. Allix, S. Chenu, E. Véron, T. Poumeyrol, E.A. Kouadri-Boudjelthia, S. Alahraché, F. Porcher, D. Massiot, F. Fayon, Considerable Improvement of Long-Persistent Luminescence in Germanium and Tin Substituted $ZnGa_2O_4$, Chem. Mater. 25(9) (2013) 1600-1606.

[41] A. Bessiere, S. Jacquart, K. Priolkar, A. Lecointre, B. Viana, D. Gourier, $ZnGa_2O_4:Cr^{3+}$: a new red long-lasting phosphor with high brightness, Opt. Express 19(11) (2011) 10131-10137.
[42] K. Tanaka, Y. Iwao, K. Hirao, N. Soga, Optical properties of transparent glass-ceramics containing $ZnGa_2O_4$-Cr^{3+} microcrystal, Bulletin of the Institute for Chemical Research 72(2) (1994) 124-133.
[43] E. Arroyo, B. Medrán, V. Castaing, G. Lozano, M. Ocaña, A.I. Becerro, Persistent luminescence of transparent $ZnGa_2O_4:Cr^{3+}$ thin films from colloidal nanoparticles of tunable size, Journal of Materials Chemistry C 9(13) (2021) 4474-4485.
[44] G. Anoop, K.M. Krishna, M.K. Jayaraj, Influence of a dopant source on the structural and optical properties of Mn doped $ZnGa_2O_4$ thin films, Applied Physics a-Materials Science & Processing 90(4) (2008) 711-715.
[45] L.-C. Tien, C.-C. Tseng, Y.-L. Chen, C.-H. Ho, Direct vapor transport synthesis of $ZnGa_2O_4$ nanowires with superior photocatalytic activity, J. Alloys Compd. 555 (2013) 325-329.
[46] V. Castaing, Research of new colours and morphologies in persistent luminescence materials, PhD Thesis - Université Paris sciences et lettres, 2019.
[47] V. Petricek, M. Dusek, L. Palatinus, Crystallographic Computing System JANA2006: General features, Zeitschrift für Kristallographie. Crystalline materials 229(5) (2014) 345-352.
[48] H. Yang, X. Qin, J. Zhang, J. Ma, D. Tang, S. Wang, Q. Zhang, The effect of MgO and SiO_2 codoping on the properties of Nd:YAG transparent ceramic, Opt. Mater. 34(6) (2012) 940-943.
[49] L. Basyrova, R. Maksimov, V. Shitov, M. Baranov, V. Mikhaylovsky, A. Khubetsov, O. Dymshits, X. Mateos, P. Loiko, Effect of SiO_2 addition on structural and optical properties of $Yb:Lu_3Al_5O_{12}$ transparent ceramics based on laser ablated nanopowders, J. Alloys Compd. 806 (2019) 717-725.
[50] S. Kochawattana, A. Stevenson, S.-H. Lee, M. Ramirez, V. Gopalan, J. Dumm, V.K. Castillo, G.J. Quarles, G.L. Messing, Sintering and grain growth in SiO_2 doped Nd:YAG, J. Eur. Ceram. Soc. 28(7) (2008) 1527-1534.
[51] J. Hostaša, F. Picelli, S. Hříbalová, V. Nečina, Sintering aids, their role and behaviour in the production of transparent ceramics, Open Ceramics 7 (2021) 100137.
[52] C. Sallé, A. Maître, J.-F. Baumard, Y. Rabinovitch, A First Approach of Silica Effect on the Sintering of Nd:YAG, Optical Review 14(4) (2007) 169-172.
[53] K. Morita, B.-N. Kim, H. Yoshida, K. Hiraga, Y. Sakka, Distribution of carbon contamination in $MgAl_2O_4$ spinel occurring during spark-plasma-sintering (SPS) processing: I – Effect of heating rate and post-annealing, J. Eur. Ceram. Soc. 38(6) (2018) 2588-2595.
[54] A. Bertrand, J. Carreaud, G. Delaizir, J.-R. Duclère, M. Colas, J. Cornette, M. Vandenhende, V. Couderc, P. Thomas, A Comprehensive Study of the Carbon Contamination in Tellurite Glasses and Glass-Ceramics Sintered by SPS, J. Am. Ceram. Soc. 97(1) (2014) 163-172.
[55] K. Morita, B.-N. Kim, H. Yoshida, K. Hiraga, Y. Sakka, Distribution of carbon contamination in oxide ceramics occurring during spark-plasma-sintering (SPS) processing: II - Effect of SPS and loading temperatures, J. Eur. Ceram. Soc. 38(6) (2018) 2596-2604.
[56] K. Morita, B.-N. Kim, H. Yoshida, K. Hiraga, Y. Sakka, Influence of pre- and post-annealing on discoloration of $MgAl_2O_4$ spinel fabricated by spark-plasma-sintering (SPS), J. Eur. Ceram. Soc. 36(12) (2016) 2961-2968.
[57] Y. Abe, D.E. Clark, Determination of combined water in glasses by infrared spectroscopy, J. Mater. Sci. Lett. 9(2) (1990) 244-245.
[58] A.M. Efimov, V.G. Pogareva, IR absorption spectra of vitreous silica and silicate glasses: The nature of bands in the 1300 to 5000 cm^{-1} region, Chem. Geol. 229(1) (2006) 198-217.
[59] J. Liu, W. Yao, B. Kear, A.K. Mukherjee, Microstructure and IR transmittance of yttria–magnesia (50:50vol.%) nano-composites consolidated from agglomerated and ultrasonic horn treated nano-powders, Materials Science and Engineering: B 171(1) (2010) 149-154.
[60] M. Suárez, A. Fernández, J.L. Menéndez, R. Torrecillas, Transparent Yttrium Aluminium Garnet Obtained by Spark Plasma Sintering of Lyophilized Gels, Journal of Nanomaterials 2009 (2009) 138490.